Electronic Supplementary Material (ESI) for Physical Chemistry Chemical Physics.

Low-Pressure and Nascent Yields of Stabilized Criegee Intermediates CH_2OO and CH_3CHOO in Ozonolysis of Propene

Lei Yang, Mixtli Campos-Pineda,[§] Katia Hatem, and Jingsong Zhang[*]

Department of Chemistry

University of California, Riverside

Riverside, CA 92521

USA

[§] Present address: Centre for Research into Atmospheric Chemistry, University College Cork, T12 YN60, Ireland.

* Corresponding author. Email: jingsong.zhang@ucr.edu; Tel +1 951 827 4197; Fax: +1 951 827 4713. Also at Air Pollution Research Center, University of California, Riverside, California 92521, United States.

Supplementary Information

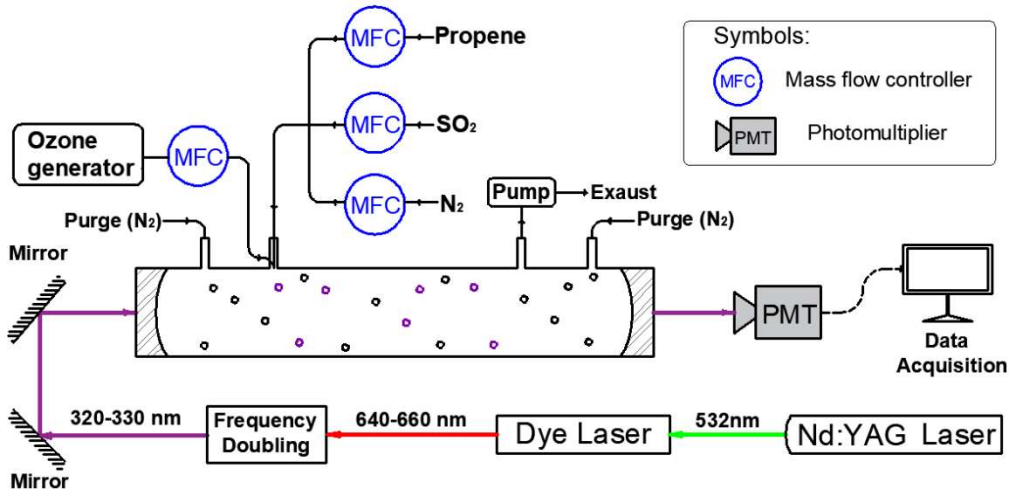

Figure S1. Experimental setup. The laser intensity into the cavity was ensured to be lower than 0.1 mJ/pulse.

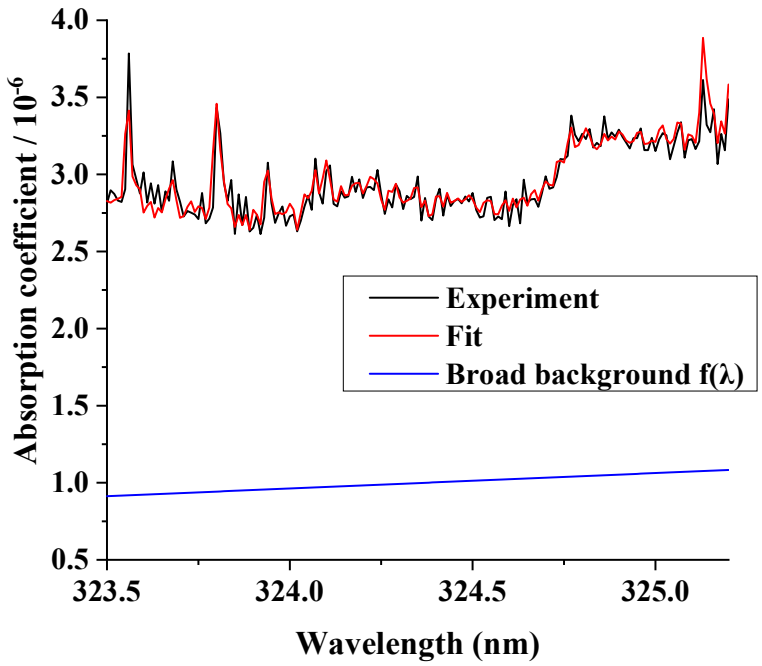

Figure S2. Illustration of the broad background $f(\lambda)$ in the representative spectra of ozonolysis (propene + O_3) in Figure 1.

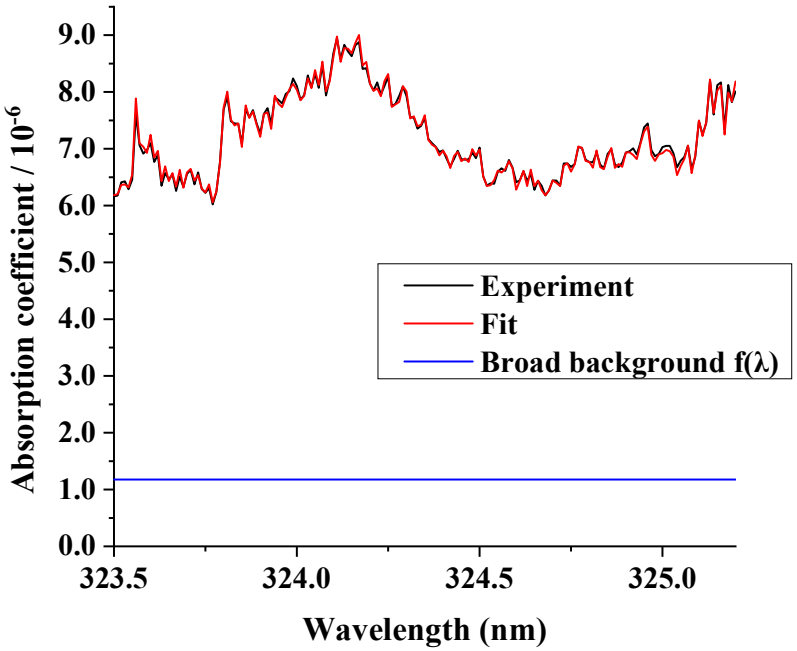

Figure S3. Illustration of the broad background f(λ) in the representative spectra of the titration reaction (propene + O_3 + SO_2) in Figure 1.

As shown Figure S2 and S3, linear functions are used in the fitting to the spectra of ozonolysis (propene + O_3) and the titration reaction (propene + O_3 + SO_2) to represent the broad absorption from unidentified species ($f(\lambda)$ in Equation 1 in main text), and to help obtain the best fit of the concentrations of O_3, SO_2 and HCHO. The slopes of these linear functions are usually very small or close to zero. The broad background in Figure S2 comes from the absorption by species produced in ozonolysis such as CH_2OO, CH_3CHOO, and CH_3CHO, yet hard to be quantified due to their small contributions and thus the lack of identifiable features in these species. More species contribute to the broad absorption in Figure S3 due to addition of SO_2 (although much less or no contribution from CIs). This illustration also explains why the experiment with the SO_2 titration is better performed at short residence time in our system. A longer reaction time would increase the accumulation of the secondary products and potentially aerosols in our system, and thus lead to an increase in the broad background absorption $f(\lambda)$ in the UV spectra. Thus, to quantify the concentrations of O_3, SO_2 and HCHO accurately, short residence time is needed to keep $f(\lambda)$ and its slope small.

Table S1. Flow parameters of the reactor under experimental conditions. Da and Pe are the Damkoehler and Péclet numbers, respectively. The radial diffusion in the flow cell can be ignored under the experimental conditions and the flow reactor can be reasonably considered and modelled as a plug flow reactor (PFR).

Characteristic Time	**Value**	**Description**	
$\mathbf{t_{ck}}$	0.1	Chemical reaction	
$\mathbf{t_{sd,R}}$	0.038	Radial species diffusion	
$\mathbf{t_{fc,R}}$	0.06	Radial forced convection	
$\mathbf{t_{fc,L}}$	3	Axial forced convection	
Negligible Axial Diffusion			
Parameter	Value	Description	Criterion*
$\mathbf{(t_{fc,R})^2/(\ t_{sd,R}\ x\ t_{ck})}$	0.01	Da/Pe^2	< 0.1
$\mathbf{t_{fc,R}/\ t_{sd,R}}$	1.6	Pe^{-1}	< 0.06
$\mathbf{t_{ck}/\ t_{fc,L}}$	0.06	Reaction time v longitudinal convection	<< 1
Negligible Poiseuille Flow			
$\mathbf{t_{sd,R}/\ t_{fc,R}}$	0.6	Pe	< 100
$\mathbf{t_{sd,R}/\ t_{fc,L}}$	0.012	Radial diffusion mixing along the reactor	< 0.5
$\mathbf{t_{sd,R}/\ t_{ck}}$	4×10^{-3}	Da	< 1
$\mathbf{t_{fc,R}/\ t_{fc,L}}$	6×10^{-3}	Da/Pe	< 0.05

*Criteria from Cutler et al.[1] and references therein.

Table S2. Kinetic modelling using the Kintecus simulation software for the propene ozonolysis and titration system.[2] Reference rate coefficients, yields of products and branching ratios were summarized mainly from IUPAC[3-5] and NIST kinetic database[6] unless otherwise stated in the comments.[7-11] Due to limited literature information, several dummy products (as noted) in secondary reactions were proposed to keep chemical equations balanced. For pressure-dependent reactions, the measurements closest to our experimental pressure were selected and used here. Units of rate coefficients k are s^{-1} and cm^3 $molecule^{-1}$ s^{-1} for unimolecular and bimolecular reactions, respectively. The nascent yields of CIs and carbonyls in reaction (1) assume only CI pathways and without secondary HCHO produced, and they were varied to model the reaction network at different pressures based on the different assumptions as listed in Table S3-S5. [a]

#	k	Reaction	Comments
(1)	1.05×10^{-17}	$C_3H_6+O_3$==>$0.621HCHO+0.056CH_3CHOO$ $+0.565CH_3CHOO^*+0.197CH_2OO+0.182CH_2OO^*$ $+0.379CH_3CHO+0.00CH_3COCH_2OOH$ [a]	Symbols: Stabilized CIs: CH_2OO and CH_3CHOO; High-energy CIs: CH_2OO^* and CH_3CHOO^*; KHP: CH_3COCH_2OOH
High-energy CH_2OO^* reactions			
(2)	8.00×10^{3}	CH_2OO^*==>CO_2+H_2	Copeland et al., 2011[a]
(3)	2.00×10^{4}	CH_2OO^*==>$CO+H_2O$	
(4)	1.20×10^{3}	CH_2OO^*==>$H+HCO_2$	
(5)	3.20×10^{4}	HCO_2==>$H+CO_2$	
(6)	700	CH_2OO^*==>$0.9HCOOH+0.1HCO+0.1OH$	Hot acid pathway
(7)	8.00×10^{-15}	$CH_2OO^*+N_2$==>CH_2OO+N_2	Collisional stabilization of high-energy CH_2OO^*
stabilized CH_2OO reactions			
(8)	7.00×10^{-14}	CH_2OO+O_3==>$HCHO+O_2+O_2$	
(9)	1.80×10^{-15}	$CH_2OO+C_3H_6$==>$HCHO+CH_3CH_2CHO$	Buras et al., 2014
(10)	6.00×10^{-12}	$CH_2OO+HCHO$==>$HCOOH+HCHO$	
(11)	1.00×10^{-13}	$CH_2OO+HCHO$==>$CO+H_2O+HCHO$	
(12)	1.00×10^{-13}	$CH_2OO+HCHO$==>$HCO+OH+HCO+H$	
(13)	1.00×10^{-13}	$CH_2OO+HCHO$==>CH_3CHO+O_2	
(14)	10	CH_2OO==>$0.7HCHO_2 + 0.3HCOOH$	Chhantyal-Pun et al., 2015
(15)	10	CH_2OO==>$HHOOC$	Wall dummy
(16)	2.41×10^{-16}	CH_2OO+H_2O==>CH_4O_3	Water dummy
(17)	7.40×10^{-11}	CH_2OO+CH_2OO==>$2HCHO+O_2$	Chhantyal-Pun et al., 2015
(18)	1.10×10^{-10}	$CH_2OO+HCOOH$==>$HCOOOCH+H_2O$	Welz et al., 2014
(19)	9.50×10^{-13}	CH_2OO+CH_3CHO==>$HCHO+CH_3COOH$	Taatjes et al., 2012
(20)	1.20×10^{-12}	CH_2OO+CH_3COOH==>$C_3H_6O_4$	Dummy product
(21)	1.00×10^{-11}	$CH_2OO+HCOOOCH$==>$H_4C_3O_5$	Dummy product
(22)	3.70×10^{-11}	CH_2OO+SO_2==>$HCHO+SO_3$	

High-energy CH_3CHOO^*: *syn*- and *anti*- partitioning			
(23)	8.40×10^{4}	CH_3CHOO^*==>$C_2H_4O_2$	*Anti*-CH_3CHOO
(24)	8.40×10^{4}	CH_3CHOO^*==>$CH_2CHO + OH$	*Syn*-CH_3CHOO
(25)	8.00×10^{-15}	$CH_3CHOO^*+N_2$==>$CH_3CHOO+N_2$	collisional stabilization of high-energy CH_3CHOO^*
High-energy *Anti*-CH_3CHOO^* reactions			
(26)	6.60×10^{4}	$C_2H_4O_2$==>$CH_2CO + H_2O$	
(27)	1.16×10^{5}	$C_2H_4O_2$==>$CH_3OH + CO$	
(28)	1.83×10^{5}	$C_2H_4O_2$==>$CH_4 + CO_2$	
(29)	2.50×10^{5}	$C_2H_4O_2$==>$CH_3CO + OH$	
(30)	2.05×10^{5}	$C_2H_4O_2$==>$CH_3 + CO_2 + H$	
Vinoxy radical reactions			
(31)	1.65×10^{-14}	$CH_2CHO + O_2$ ==> $CHOCHO + OH$	
(32)	5.50×10^{-15}	$CH_2CHO + O_2$ ==> $HCHO + CO + OH$	
(33)	4.40×10^{-14}	$CH_2CHO + O_2$ ==> $CH_2CO + HO_2$	
(34)	4.40×10^{-14}	$CH_2CHO + O_2$ ==> $OOCH_2CHO$	
(35)	10	CH_2CHO==> $OHCH_2C$	Wall dummy
Stabilized CH_3CHOO reactions			
(36)	10	CH_3CHOO==>$HHCCOOHH$	Wall dummy
(37)	160	CH_3CHOO==>$CH_2CHO + OH$	
(38)	1.10×10^{-12}	$CH_3CHO+CH_3CHOO$==>$C_4H_8O_3$	$C_4H_8O_3$ is SOZ
(39)	2.60×10^{-14}	$CH_3CHO+CH_3CHOO$==>$CH_3COOH+CH_3CHO$	
(40)	3.60×10^{-15}	$CH_3CHO+CH_3CHOO$==>$H_2O+HCHO+HCHO + H_2C_2$	
(41)	7.00×10^{-14}	$CH_3CHOO+O_3$==>$CH_3CHO+O_2+O_2$	Estimated from k(CH_2OO+O_3)
(42)	4.00×10^{-18}	$CH_3CHOO+H_2O$==>$C_2H_6O_3$	Dummy
(43)	1.50×10^{-15}	$CH_3CHOO + C_3H_6$ ==> $CH_3CHO + CH_3CH_2CHO$	Dummy
(44)	6.00×10^{-12}	$CH_3CHOO+HCHO$==>$C_3H_6O_3$	$C_3H_6O_3$ is SOZ
(45)	1.00×10^{-11}	$CH_3CHOO+CH_2CHO$==>$CH_3CHOOCH_2CHO$	Dummy
(46)	1.10×10^{-10}	$CH_3CHOO+HCOOH$==>$CH_3COOOCH+H_2O$	Estimated from k($CH_2OO+HCOOH$)
(47)	9.50×10^{-13}	$CH_3CHOO+CH_3CHO$==>$CH_3CHO+CH_3COOH$	Estimated from k(CH_2OO+CH_3CHO)
(48)	1.20×10^{-12}	$CH_3CHOO+CH_3COOH$==>$C_4H_8O_4$	Estimated from k(CH_2OO+CH_3COOH)
(49)	2.60×10^{-11}	$CH_3CHOO+SO_2$==>$CH_3CHO+SO_3$	2.60×10^{-11} for *syn*-CH_3CHOO and 1.40×10^{-10} for *anti*-CH_3CHOO
Secondary reactions of O_3			
(50)	2.66×10^{-11}	$H+O_3$==>$OH+O_2$	
(51)	9.13×10^{-13}	$O_3+HOCH_2CH_2$==>$HCHO+CH_2OH+O_2$	
(52)	9.13×10^{-13}	O_3+CH_2OH==>$HCHO+OH+O_2$	
(53)	7.30×10^{-14}	$OH+O_3$==>HO_2+O_2	
(54)	2.00×10^{-15}	HO_2+O_3==>$OH+2O_2$	
(55)	8.00×10^{-15}	$O+O_3$==>$2O_2$	

Secondary reactions of propene			
(56)	1.57×10^{-12}	$C_3H_6+H==>C_3H_7$	
(57)	5.00×10^{-13}	$C_3H_7+O_2==>C_3H_6+HO_2$	
(58)	1.10×10^{-11}	$C_3H_7+O_2==>CH_3CHO_2CH_3$	
(59)	2.90×10^{-11}	$C_3H_6+OH==>C_3H_6OH$	Scavenge OH
HO_x reactions (non VOC)			
(60)	5.60×10^{-12}	$H+HO_2==>H_2+O_2$	
(61)	7.20×10^{-11}	$H+HO_2==>2OH$	
(62)	2.40×10^{-12}	$H+HO_2==>H_2O+O$	
(63)	3.50×10^{-11}	$O+OH==>O_2+H$	
(64)	5.80×10^{-11}	$O+HO_2==>OH+O_2$	
(65)	1.70×10^{-15}	$O+H_2O_2==>OH+HO_2$	
(66)	6.70×10^{-15}	$H_2+OH==>H_2O+H$	
(67)	1.48×10^{-12}	$OH+OH==>H_2O+O$	
(68)	2.60×10^{-13}	$OH+OH==>H_2O_2$	Pressure dependent
(69)	1.10×10^{-10}	$OH+HO_2==>H_2O+O_2$	
(70)	1.70×10^{-12}	$OH+H_2O_2==>H_2O+HO_2$	
(71)	1.60×10^{-12}	$HO_2+HO_2==>H_2O_2+O_2$	Pressure dependent
Secondary reactions of O_2			
(72)	1.27×10^{-14}	$H+O_2==>HO_2$	Pressure dependent
(73)	1.80×10^{-16}	$O+O_2==>O_3$	Pressure dependent
(74)	5.20×10^{-12}	$HCO+O_2==>CO+HO_2$	
(75)	5.10×10^{-12}	$CH_3CO+O_2==>CH_3COOO$	Pressure dependent
HO_x reactions with VOC			
(76)	1.44×10^{-13}	$OH+CO==>H+CO_2$	
(77)	8.50×10^{-12}	$OH+HCHO==>H_2O+HCO$	
(78)	1.43×10^{-11}	$OH+CH_3CHO==>H_2O+CH_3CO$	
(79)	7.50×10^{-13}	$OH+CH_3CHO==>H_2O+CH_2CHO$	
(80)	4.50×10^{-13}	$OH+HCOOH==>CH_3O_3$	Dummy
(81)	7.90×10^{-14}	$HO_2+HCHO==>HOCH_2OO$	
(82)	150	$HOCH_2OO==>HO_2+HCHO$	
(83)	7.00×10^{-13}	$HOCH_2OO+HOCH_2OO==>HCOOH+CH_2OHOH+O_2$	
(84)	5.50×10^{-12}	$HOCH_2OO+HOCH_2OO==>2HOCH_2O+O_2$	
(85)	6.00×10^{-12}	$HO_2+HOCH_2OO==>O_2+HOCH_2O_2H$	
(86)	4.00×10^{-12}	$HO_2+HOCH_2OO==>O_2+HCOOH+H_2O$	
(87)	2.00×10^{-12}	$HO_2+HOCH_2OO==>O_2+OH+HOCH_2O$	
(88)	7.74×10^{-13}	$CH_3OH + OH ==> 0.85CH_2OH + 0.85H_2O +0.15CH_3O+0.15H_2O$	
(89)	1.00×10^{-11}	$OH+CH_2CHO==>OHCH_2CHO$	Dummy
Decomposition reactions of KHP			
(90)	10	$CH_3COCH_2OOH==>CH_3COCHO+H_2O$	Estimated rates
(91)	10	$CH_3COCH_2OOH==>CH_3COCHO+OH+H$	Estimated rates
(92)	10	$CH_3COCH_2OOH==>HCO+CH_3CHO+OH$	Estimated rates
(93)	10	$CH_3COCH_2OOH==>CH_3CO+HCHO+OH$	Estimated rates

[a] Specifically, the yields of KHP and secondary HCHO have not been well established to date, thus we used a few assumptions based on previous studies on ethene ozonolysis. The corresponding yields of CIs and carbonyls will be affected and are summarized in Table S3.

Table S3. Summary on the nascent yields of CIs based on different assumptions in ozonolysis of propene.

		Assumptions [a]				Summary
		Only CI pathways and no secondary HCHO	5% secondary HCHO from bimolecular reactions of CH_2OO [b]	12% KHP [c]	12% KHP, and 5% secondary HCHO from bimolecular reactions of CH_2OO	
POZ branching	Primary CH_3CHO	38 ± 5%	43 ± 5%	29 ± 5%	34 ± 5%	29-43%
	Primary HCHO	62 ± 5%	57 ± 5%	59 ± 5%	54 ± 5%	54-62%
High-energy CI and sCI branching	Total sCI	25 ± 2%	25 ± 2%	25 ± 2%	25 ± 2%	25%
	Total high-energy CI	75 ± 2%	75 ± 2%	63 ± 2%	63 ± 2%	63-75%
CI branching ratios	High-energy CH_2OO	18 ± 5%	18 ± 5%	9 ± 5%	9 ± 5%	9-18%
	High-energy CH_3CHOO	57 ± 5%	57 ± 5%	53 ± 5%	54 ± 5%	53-57%
	Stabilized CH_2OO	20 ± 2%	25 ± 2%	20 ± 2%	25 ± 2%	20-25%
	Stabilized CH_3CHOO	5 ± 2%	0 ± 2%	5 ± 2%	0 ± 2%	0-5%
Stabilization factor	CH_2OO	52%	59%	68%	74%	52-74%
	CH_3CHOO	9%	0%	9%	0%	0-9%

a. Assumptions

In Table S3, the possible error sources that affect our measurements on primary HCHO yields and corresponding CI/carbonyl yields are listed and discussed below. It should be noted that the total yield of sCI ($\Delta[SO_2]/\Delta[O_3]$) is not affected by these assumptions to the authors' knowledge (more discussion in the main text).

b. Secondary HCHO produced from bimolecular reactions of CH_2OO.

The primary HCHO yield measured in this work could be overestimated. According to the previous reported yield of total carbonyls of 100-110%, the overestimation could be 0-10%, because of the secondary HCHO potentially produced from CH_3CHOO or KHP decomposition or from the bimolecular reactions between CH_2OO and O_3, propene, CH_3CHO, etc. (as listed in Table S4). Short residence times of < 1s were used in this work to suppress the production of secondary organic acids and carbonyls, yet the other pathways of secondary HCHO may not be omitted and should be further investigated, as discussed below.

Our kinetic model can help evaluate how much overestimation there could be due to the bimolecular reactions of CH_2OO. By setting the initial concentration of SO_2 to be zero and keeping the other conditions the same (using the same kinetic model in Table S2 with residence time ~0.92 s, $[O_3]_i \sim 1.5 \times 10^{14}$, $[\text{propene}]_i \sim 1.0 \times 10^{17}$), the kinetic model predicts the yield of HCHO to be ~70% (higher than the 62% primary HCHO yield), indicating ~8% secondary HCHO from the other pathways. Thus, we can use the kinetic model to help find the actual value of the primary HCHO yield. We vary the primary HCHO and CH_3CHO yield in the model. When setting the primary HCHO yield to be 54%, the resultant HCHO yield is the same as the HCHO yield measured by our experiment, 62% (meaning 54% of primary HCHO and 8% secondary HCHO). Since the current model assumes the HCHO channel to be 100% for the reactions listed in Table S4, this 8% should be considered an upper limit of the secondary HCHO yield. To further investigate the pathways producing the secondary HCHO from CH_2OO, relevant reactions of CH_2OO are listed in Table S4, together with the calculated average concentrations of the reactants and the pseudo-first-order reaction rates. Since the secondary HCHO produced from the reaction CH_2OO + HCHO does not change the HCHO concentrations, the major contributing factors for secondary HCHO production in our system is the reaction between CH_2OO and propene with a pseudo-first-order reaction rate of 179 s^{-1} (contributing ~7% extra HCHO), due to the high concentration of propene used in the experiments. The reaction between CH_2OO and CH_3CHO also contributed ~1% secondary HCHO generation in our experiments.

In the meantime, secondary HCHO produced from bimolecular reactions between CH_2OO and other molecules before adding SO_2 will affect the measurements of the yield of stabilized CH_2OO in this work. Specifically, the reactions such as $CH_2OO + C_3H_6$ already converts part of CH_2OO into HCHO before adding SO_2. The secondary HCHO yield after adding SO_2 (quantified by $\Delta[\text{HCHO}] = [\text{HCHO}]_f - [\text{HCHO}]_i$) may underestimate the yield of stabilized CH_2OO. Thus, the 20% nascent yield of stabilized CH_2OO from $\Delta[\text{HCHO}]/\Delta[O_3]$ should be considered as the lower limit of the stabilized CH_2OO yield. On the other hand, total nascent yield of sCIs from $\Delta[SO_2]/\Delta[O_3]$ (25%) sets an upper limit of stabilized CH_2OO yield. Thus, stabilized CH_2OO yield is 20-25%, and the secondary HCHO from bimolecular reactions of CH_2OO in ozonolysis would not be higher than 5%. This is lower than the 8% estimated from the kinetic model, probably due to other possible product channels of CH_2OO's bimolecular reactions (for example, $CH_2OO + C_3H_6$ may also produces hydroperoxides).[13]

Therefore, considering the results from both our kinetic modelling as well as the $\Delta[\text{HCHO}]/\Delta[O_3]$ and $\Delta[SO_2]/\Delta[O_3]$ measured in this work, the yield of secondary HCHO from CH_2OO bimolecular reaction before adding SO_2 should be $\leq 5\%$.

c. KHP pathways and secondary HCHO produced from KHP decomposition.

There could also be some extra secondary HCHO produced from ketohydroperoxide (KHP) decomposition. There is experimental evidence performed in ethene ozonolysis showing that the POZ can decompose to form 2-hydroperoxyacetaldehyde (HPA), a type of ketohydroperoxide (KHP),[14] which could further decompose through pathways including glyoxal + H_2O, glyoxal + OH + H, and HCO + HCHO + OH.[15] The observation of glyoxal in ethene ozonolysis has been confirmed by experiment,[16] yet exact branching ratios are still unknown. Although there are no similar studies on propene ozonolysis reported yet, a similar mechanism could potentially add sources to the secondary HCHO production. The branching into KHP and the secondary HCHO potentially produced from KHP decomposition will not affect the measurements on the sCI yields or the stabilized CH_2OO yields, but it may influence the measurements on the primary HCHO yield and thus affect the calculations on the high-energy CI

branching ratios.

To evaluate the effect on the secondary HCHO production, the reactions of KHP are added to our kinetic model (Reaction (90)-(93) in Table S2). Assuming the same pathways as in ethene ozonolysis, KHP (CH_3COCH_2OOH and $HOOCH(CH_3)CHO$) formed in propene ozonolysis could finally decompose to methylglyoxal (CH_3COCHO) + H_2O, methylglyoxal + OH + H, HCO + CH_3CHO + OH, or CH_3CO + HCHO + OH (the last pathway potentially generates secondary HCHO).

In ozonolysis, the chemistry involved with KHP is still not well known and the decomposition rates and branching ratios remain undetermined. In our kinetic model, the yield of KHP in propene + O_3 reaction is assumed to be the same as in ethene ozonolysis (12%).[12] We also assume equal branching ratios among the four decomposition pathways of KHP (each ~3%). A total rate constant of 40 s^{-1} is fast enough for all KHP to decompose within the residence time of our experiments (0.92 s). From the kinetic modelling results, the yield of HCHO increased by ~3% compared to the previous models, indicating ~3% extra amount of secondary HCHO produced from the KHP decomposition. Varying the branching ratios by increasing the CH_3CO + HCHO + OH channel to the upper limit of 12% (removing the other pathways) would result in ~12% increase in HCHO yield, yet this is likely not the real case since glyoxal was observed in experimental studies in ethene ozonolysis.[16] As suggested by Lewin et al.[16] and Genossar et al.[15] "…decomposition of HPA would mainly lead to the formation of glyoxal…". Thus, we use the equivalent branching in our kinetic models to estimate the secondary HCHO produced from KHP.

As Lewin et al.[16] suggested "…The decomposition of HPA must occur within the ∼1 minute residence time but as HPA is detected, the reaction is not very fast either…", the total rate constant of 40 s^{-1} used here might be an upper limit. The shorter residence time ~0.92 s used in our experiments (compared to the 1-minute residence time used by Lewin et al.[16]) may further suppress the secondary HCHO production from the decomposition of KHP, depending on how fast the decomposition reaction of KHP actually is. A rough estimation can be made based on the reported KHP measurements and our kinetic model. In the experimental work by Rousso et al,[14] KHP (HPA) was observed and its concentration was estimated to be ~5 ppm from the ozonolysis of ethene at conditions near atmospheric pressure (~700 Torr) and temperature (~300 K) with a residence time of 1.3 s. By adding the reactions of KHP listed in Table S5 to the reaction network of ethene ozonolysis reported in our previous work,[17] the KHP concentration can be modelled by varying its decomposition rate coefficients (assuming KHP yield is 12% and an equivalent branching between the three decomposition pathways of KHP). With the initial concentrations of ethene, O_3, O_2 and argon set to be 4.48×10^{17}, 2.24×10^{16}, 2.66×10^{18}, and 1.92×10^{19} molecules cm^{-3} (corresponding to the 2% ethene, 1000 ppm O_3, 12% O_2 and 86% argon used by Rousso et al.[14]), the best agreement between the revised ethene ozonolysis model and the reported 5 ppm concentration of KHP is when the total decomposition rate of KHP is set to be 7.5 s^{-1}. Although the plug flow reactor kinetic model and steady-state estimation used here may not be perfect for their instrument (depending on the specific parameters of their flow reactor), this result indicates that the rate coefficients that we use in the propene ozonolysis should be large enough for the decomposition reactions of KHP.

In sum, the evaluation on the overestimation of the primary HCHO yield was performed by the kinetic modelling and a few assumptions as listed in Table S3. Our current model suggests that among the observed 62% HCHO yield in propene ozonolysis, up to 5% can come from the bimolecular reactions between CH_2OO and propene or CH_3CHO, and ~3% from the KHP decomposition pathway. This upper limit of ~8% of extra HCHO production is consistent with the previous studies that measured the total carbonyl yields to be 100-110% in propene ozonolysis.[18, 19] Thus, the actual primary HCHO yield should be in the range of 54-62%.

Based on all these estimations/assumptions, the measured CI and carbonyl yields can also be corrected as summarized in Table S3. The ranges of these yields are reported as the results in the main text.

Table S4. Secondary HCHO production reactions in bimolecular reactions of CH_2OO.

Rate constant k (cm^3 $molecule^{-1}$ s^{-1})	Reaction (CH_2OO + X)	Average concentration of X (molecules cm^{-3})	Pseudo-first-order reaction rates k[X] (s^{-1})
7.00×10^{-14}	CH_2OO+O_3==>$HCHO+O_2+O_2$	9.29×10^{13}	7
1.80×10^{-15}	$CH_2OO+C_3H_6$==>$HCHO+CH_3CH_2CHO$	9.95×10^{16}	179
7.40×10^{-11}	CH_2OO+CH_2OO==>$2HCHO+O_2$	3.74×10^{10}	3
9.50×10^{-13}	CH_2OO+CH_3CHO==>$HCHO+CH_3COOH$	2.61×10^{13}	25
6.00×10^{-12}	$CH_2OO+HCHO$==>$HCOOH+HCHO$	3.50×10^{13}	210
1.00×10^{-13}	$CH_2OO+HCHO$==>$CO+H_2O+HCHO$	3.50×10^{13}	3

Table S5. Production and decomposition reactions of KHP in ethene ozonolysis.

k (s^{-1} for unimolecular, cm^3 $molecule^{-1}$ s^{-1} for bimolecular reactions)	Reactions
1.60×10^{-18}	$C_2H_4+O_3$==>$0.88HCHO+0.201CH_2OO+0.679CH_2OO^*$ $+0.12HOOCH_2CHO$
2.5	$HOOCH_2CHO$==>$HCHO+HCO+OH$
2.5	$HOOCH_2CHO$==>$CHOCHO+OH+H$
2.5	$HOOCH_2CHO$==>$CHOCHO+H_2O$

Table S6. The total yield of sCIs in ozonolysis of propene measured from 7 to 16 Torr.

Total pressure, Torr	$\Delta[SO_2]//[\Delta O_3]$	Total pressure, Torr	$\Delta[SO_2]//[\Delta O_3]$
7	30.9%	13	31.3%
7	20.6%	13	22.4%
7	26.5%	13	26.9%
10	27.5%	13	32.8%
10	24.6%	13	23.9%
10	30.4%	13	25.4%
10	26.1%	16	31.0%
10	26.1%	16	25.9%
10	26.1%	16	25.9%

When making the linear fit y = a + bx to extrapolate the zero-pressure nascent yield of sCI, the least-squares method (method of maximum likelihood) is used (see Bevington, P. R.; Robinson, D. K. *Data Reduction and Error Analysis for the Physical Sciences* 3rd ed., McGraw-Hill, Inc., New York, 2003).[20] The following is the calculation procedure.

The sCI yield data and error bars at each pressure calculated from Table S6 are listed below.

Pressure in Torr (x_i)	sCI yield (y_i)	sCI yield error (σ_i)
7	0.260	0.052
10	0.268	0.020
13	0.271	0.042
16	0.276	0.030

$$\text{Intercept } a = \frac{\sum\frac{x_i^2}{\sigma_i^2}\sum\frac{y_i}{\sigma_i^2} - \sum\frac{x_i}{\sigma_i^2}\sum\frac{x_i y_i}{\sigma_i^2}}{\sum\frac{1}{\sigma_i^2}\sum\frac{x_i^2}{\sigma_i^2} - \left(\sum\frac{x_i}{\sigma_i^2}\right)^2} = 0.253 \approx 25\%$$

$$\text{Slope } b = \frac{\sum\frac{1}{\sigma_i^2}\sum\frac{x_i y_i}{\sigma_i^2} - \sum\frac{x_i}{\sigma_i^2}\sum\frac{y_i}{\sigma_i^2}}{\sum\frac{1}{\sigma_i^2}\sum\frac{x_i^2}{\sigma_i^2} - \left(\sum\frac{x_i}{\sigma_i^2}\right)^2} = 0.00148$$

$$\text{Reduced chi} - \text{square } \chi_v^2 = \frac{\sum\left(\frac{y_i - a - bx_i}{\sigma_i}\right)^2}{N-2} = 0.00271$$

This $\chi_v^2 < 1$, indicating that the errors of the data points are overestimated, and the uncertainties of the data points could be revised by a factor of χ_v^2 (see Chapter 6, Bevington and Robinson). Consequently, the uncertainly of the intercept σ_a is revised to $\sigma_a{}'$ as shown in the following:

$$\text{Standard error of intercept } \sigma_a' = \left[\chi_\nu^2 \frac{\sum \frac{x_i^2}{\sigma_i^2}}{\sum \frac{1}{\sigma_i^2} \sum \frac{x_i^2}{\sigma_i^2} - \left(\sum \frac{x_i}{\sigma_i^2} \right)^2} \right]^{\frac{1}{2}} = 0.322\%$$

For a two-tailed *t*-test at 95% confidence level, the *t*-value is 4.303 when the degree of freedom ν is 2, and thus, the error bar of the intercept at 95% confidence level is:

$$t_{95\%} \times \sigma_a{}' \approx 2\%$$

The intercept has a smaller error bar (2%) than the error bars of the 7-16 Torr data points (2-5%) mainly because:

(1) in a weighted linear fit with the method of maximum likelihood, the data points with larger error bars have lower weighting factors and less contribution to the slope and the intercept of the linear fit. Consequently, the data points at 7 and 13 Torr with error of 4-5% contribute less than those at 10 and 16 Torr, and the overall error of the y-intercept in the fitting is closer to the errors of these points (about 2%). Furthermore, the uncertainty of the y-intercept of a linear fit could be in general smaller than those of individual data points due to their collective contributions.

(2) the goodness-of-fit parameter, the chi-square, is of a low value. The reduced chi-square χ_ν^2 of 0.00271 shows that the fitting is of high probability over 99% according to the χ^2 distribution (referred to Table C.4 on page 256 of the Bevington and Robinson reference book). Alternatively, this small $\chi_\nu^2 (< 1)$ indicates that the errors of the data points are overestimated, and the uncertainties of the data points could be revised by a factor of χ_ν^2 (Chapter 6, Bevington and Robinson). This helps reduce the error bar of the intercept.

Table S7. The yield of stabilized CH_2OO in ozonolysis of propene measured from 7 to 16 Torr.

Total pressure, Torr	Δ[HCHO]/$\Delta[O_3]$	Total pressure, Torr	Δ[HCHO]/$\Delta[O_3]$
7	19.1%	13	20.9%
7	19.1%	13	22.4%
7	23.5%	13	20.9%
10	18.8%	13	20.9%
10	20.3%	13	22.4%
10	21.7%	13	22.4%
10	23.2%	16	22.4%
10	20.3%	16	22.4%
10	21.7%	16	20.7%

The least-squares method (method of maximum likelihood) is used when making the linear fit y = a + bx to extrapolate the zero-pressure nascent yield of stabilized CH_2OO.[20] The following is the calculation procedure.

The stabilized CH_2OO yield data and error bars at each pressure calculated from Table S7 are listed below.

Pressure in Torr (x_i)	sCI yield (y_i)	sCI yield error (σ_i)
7	0.206	0.025
10	0.210	0.011
13	0.216	0.008
16	0.218	0.010

$$\text{Intercept } a = \frac{\sum\frac{x_i^2}{\sigma_i^2}\sum\frac{y_i}{\sigma_i^2} - \sum\frac{x_i}{\sigma_i^2}\sum\frac{x_i y_i}{\sigma_i^2}}{\sum\frac{1}{\sigma_i^2}\sum\frac{x_i^2}{\sigma_i^2} - \left(\sum\frac{x_i}{\sigma_i^2}\right)^2} = 0.197 \approx 20\%$$

$$\text{Slope } b = \frac{\sum\frac{1}{\sigma_i^2}\sum\frac{x_i y_i}{\sigma_i^2} - \sum\frac{x_i}{\sigma_i^2}\sum\frac{y_i}{\sigma_i^2}}{\sum\frac{1}{\sigma_i^2}\sum\frac{x_i^2}{\sigma_i^2} - \left(\sum\frac{x_i}{\sigma_i^2}\right)^2} = 0.00140$$

$$\text{Reduced chi} - \text{square } \chi_v^2 = \frac{\sum\left(\frac{y_i - a - bx_i}{\sigma_i}\right)^2}{N-2} = 0.0199$$

This $\chi_v^2 < 1$, indicating that the errors of the data points are overestimated, and the uncertainties of the data points could be revised by a factor of χ_v^2 (see Chapter 6, Bevington and Robinson). Consequently, the uncertainly of the intercept σ_a is revised to $\sigma_a{}'$ as shown in the following:

$$\text{Standard error of intercept } \sigma_a' = \left[\chi_v^2 \frac{\sum \frac{x_i^2}{\sigma_i^2}}{\sum \frac{1}{\sigma_i^2} \sum \frac{x_i^2}{\sigma_i^2} - \left(\sum \frac{x_i}{\sigma_i^2} \right)^2} \right]^{\frac{1}{2}} = 0.395\%$$

For a two-tailed *t*-test at 95% confidence level, the *t*-value is 4.303 when the degree of freedom ν is 2, and thus, the error bar of the intercept at 95% confidence level is:

$$t_{95\%} \times \sigma_a{}' \approx 2\%$$

References

1. A. H. Cutler, M. J. Antal and M. Jones, *Ind. Eng. Chem. Res.*, 1988, **27**, 691-697.
2. J. C. Ianni, in *Computational Fluid and Solid Mechanics 2003*, ed. K. J. Bathe, Elsevier Science Ltd., Oxford, 2003, pp. 1368-1372.
3. R. A. Cox, M. Ammann, J. N. Crowley, H. Herrmann, M. E. Jenkin, V. F. McNeill, A. Mellouki, J. Troe and T. J. Wallington, *Atmos. Chem. Phys.*, 2020, **20**, 13497-13519.
4. R. Atkinson, D. L. Baulch, R. A. Cox, J. N. Crowley, R. F. Hampson, R. G. Hynes, M. E. Jenkin, M. J. Rossi, J. Troe and I. Subcommittee, *Atmos. Chem. Phys.*, 2006, **6**, 3625-4055.
5. R. Atkinson, D. L. Baulch, R. A. Cox, J. N. Crowley, R. F. Hampson, R. G. Hynes, M. E. Jenkin, M. J. Rossi and J. Troe, *Atmos. Chem. Phys.*, 2004, **4**, 1461-1738.
6. J. A. Manion, R. E. Huie, R. D. Levin, J. D. R. Burgess, V. L. Orkin, W. Tsang, W. S. McGivern, J. W. Hudgens, V. D. Knyazev, D. B. Atkinson, E. Chai, A. M. Tereza, C.-Y. Lin, T. C. Allison, W. G. Mallard, F. Westley, J. T. Herron, R. F. Hampson and D. H. Frizzell, NIST Chemical Kinetics Database, NIST Standard Reference Database 17, Version 7.0 (Web Version), Release 1.6.8, Data version 2015.09, https://kinetics.nist.gov/, (accessed 1 June, 2023).
7. G. Copeland, M. V. Ghosh, D. E. Shallcross, C. J. Percival and J. M. Dyke, *Phys. Chem. Chem. Phys.*, 2011, **13**, 14839.
8. R. Chhantyal-Pun, A. Davey, D. E. Shallcross, C. J. Percival and A. J. Orr-Ewing, *Phys. Chem. Chem. Phys.*, 2015, **17**, 3617-3626.
9. O. Welz, A. J. Eskola, L. Sheps, B. Rotavera, J. D. Savee, A. M. Scheer, D. L. Osborn, D. Lowe, A. Murray Booth, P. Xiao, M. Anwar H. Khan, C. J. Percival, D. E. Shallcross and C. A. Taatjes, *Angew. Chem., Int. Ed.*, 2014, **53**, 4547-4550.
10. C. A. Taatjes, O. Welz, A. J. Eskola, J. D. Savee, D. L. Osborn, E. P. F. Lee, J. M. Dyke, D. W. K. Mok, D. E. Shallcross and C. J. Percival, *Phys. Chem. Chem. Phys.*, 2012, **14**, 10391-10400.
11. Z. J. Buras, R. M. I. Elsamra, A. Jalan, J. E. Middaugh and W. H. Green, *J. Phys. Chem. A*, 2014,

118, 1997-2006.

12. M. Pfeifle, Y. T. Ma, A. W. Jasper, L. B. Harding, W. L. Hase and S. J. Klippenstein, *J. Chem. Phys.*, 2018, **148**, 174306.
13. C. Sun, B. Xu, L. Lv and S. Zhang, *Phys. Chem. Chem. Phys.*, 2019, **21**, 16583-16590.
14. A. C. Rousso, N. Hansen, A. W. Jasper and Y. Ju, *J. Phys. Chem. A*, 2018, **122**, 8674-8685.
15. N. Genossar, J. P. Porterfield and J. H. Baraban, *Phys. Chem. Chem. Phys.*, 2020, **22**, 16949-16955.
16. C. S. Lewin, O. Herbinet, G. A. Garcia, P. Arnoux, L.-S. Tran, G. Vanhove, L. Nahon, F. Battin-Leclerc and J. Bourgalais, *Chem. Commun.*, 2022, **58**, 13139-13142.
17. L. Yang, M. Campos-Pineda and J. Zhang, *J. Phys. Chem. Lett.*, 2022, **13**, 11496-11502.
18. O. Horie and G. K. Moortgat, *Atmos. Environ.*, 1991, **25**, 1881-1896.
19. E. C. Tuazon, S. M. Aschmann, J. Arey and R. Atkinson, *Environ. Sci. Technol.*, 1997, **31**, 3004-3009.
20. P. R. Bevington and D. K. Robinson, *Data Reduction and Error Analysis for the Physical Sciences Third Edition*, McGraw-Hili, Inc., New York, 2003.